

# Hierarchical Fiber Clustering Based on Multi-scale Neuroanatomical Features

Qian Wang<sup>1,2</sup>, Pew-Thian Yap<sup>2</sup>, Hongjun Jia<sup>2</sup>, Guorong Wu<sup>2</sup>, and Dinggang Shen<sup>2</sup>

<sup>1</sup> Department of Computer Science, University of North Carolina at Chapel Hill  
qianwang@cs.unc.edu

<sup>2</sup> Department of Radiology and BRIC, University of North Carolina at Chapel Hill  
{ptyap, jiahj, grwu, dgshen}@med.unc.edu

**Abstract.** DTI fiber tractography inspires unprecedented understanding of brain neural connectivity by allowing in vivo probing of the brain white-matter microstructures. However, tractography algorithms often output hundreds of thousands of fibers and thus render the fiber analysis a challenging task. By partitioning a huge number of fibers into dozens of bundles, fiber clustering algorithms make the task of analyzing fiber pathways relatively much easier. However, most contemporary fiber clustering methods rely on fiber geometrical information only, ignoring the more important anatomical aspects of fibers. We propose in this paper a hierarchical atlas-based fiber clustering method which utilizes multi-scale fiber neuroanatomical features to guide the clustering. In particular, for each level of the hierarchical clustering, specific scaled ROIs at the atlas are first diffused along the fiber directions, with the spatial confidence of diffused ROIs gradually decreasing from 1 to 0. For each fiber, a fuzzy associativity vector is defined to keep track of the maximal spatial confidences that the fiber can have over all diffused ROIs, thus giving the anatomical signature of the fiber. Based on the associativity vectors and the ROI covariance matrix, the Mahalanobis distance between two fibers is then calculated for fiber clustering using spectral graph theory. The same procedure is iterated over coarse-to-fine ROI scales, leading to a hierarchical clustering of the fibers. Experimental results indicate that reasonable fiber clustering results can be achieved by the proposed method.

## 1 Introduction

Diffusion Tensor Imaging (DTI) is well-established for characterizing neural pathways in the brain. It allows microstructural delineation of tissue water diffusion pattern, where water molecules diffuse with more freedom along neurons but not in directions perpendicular to them. Each diffusion tensor captures a part of this diffusion pattern and the tractography algorithms allow a streamline tracing of this pattern along the tensor eigenvectors, resulting in a significant number of fibers. These fibers carry with them abundant brain water diffusivity information and thus provide a unique perspective of neural connectivity as well as the evidence of linkage between brain regions. This has enriched researchers' understanding of the internal working mechanism of the brain, both structurally and functionally.

A tractography algorithm can usually yield a very huge number of fibers, typically in the order of  $10^3$ - $10^6$ . Such massive amount of fibers often renders subsequent analysis difficult, and makes information provided by the fibers not immediately decipherable. One approach to remedy this is to parcellate tractography results so that the fibers are grouped into the related bundles. For example, fiber clustering can partition the whole tractography results into dozens of bundles, each of which contains fibers behaving similarly in structure as well as in function.

In general, regardless of the clustering method employed, fiber clustering needs the definition of a pairwise similarity/distance measure between two fibers. And most fiber clustering methods up to date rely on fiber geometric features only. In [1] for example, after point-to-point correspondence is detected along two fibers, the ratio measuring the length of the corresponding segment against the overall fiber length is calculated as the similarity measure. The correspondence ratio is highest if the two fibers are identical, and approaches zero if the pairwise correspondence is minimal. In [2], a fiber is regarded as a discrete point set in the Euclidean space, and can be described by the mean of the point set as well as the covariance. Kernel methods are then used to evaluate the fiber similarity based on their individual feature descriptors. In [3][4][5], the generic Hausdorff distance and its variations are applied. The Hausdorff distance in general computes the upper bound of the minimal point-to-point distance between two fibers. Similarity in [6] is estimated by counting the number of voxels through which both fibers are passing, while in [7] the contributions of two fibers are weighted and integrated along the shared pathway. Though no explicit pairwise similarity of fibers is defined, the methods in [8][9][10] adopt a similar strategy when determining the relationship between the fiber under consideration and other fibers (or bundles).

All methods above have in common the shortcoming of not taking into account the neuroanatomical information of fibers, which can be provided by the atlas containing specifications of manual labels. In [11][12][13] for example, information from the atlas is used to help identify detected fiber bundles, though the similarity between fibers is still defined from the geometric perspective, by viewing each fiber as a 3D trajectory only. Recently, some researchers begin introducing the more important anatomical features into fiber clustering. In [14], fibers connecting identical anatomical regions are grouped into a common bundle to reduce the workload of subsequent geometric feature based clustering. However, even though the ROIs are manually delineated by experts, the consistency of the parcellation remains in question due to inevitable bias in labeling. Furthermore, the vector pertaining to the associativity of the fiber with respect to all ROIs is sparse in that a single fiber usually relates to a very limited number of anatomical regions. Great challenges are thus brought into the estimation of pairwise fiber distances based on the anatomical features of fibers.

To solve these problems, we propose a hierarchical atlas-based fiber clustering method which utilizes multi-scale neuroanatomical fiber associativity features. In each level of the hierarchical clustering, a specific scaled ROI from the atlas is diffused along the fiber directions. A fuzzy associativity vector of each fiber is then acquired from the set of diffused ROIs. The Mahalanobis distance between fibers is calculated from their associativity vectors and further employed by spectral clustering. Performed iteratively in a hierarchy of scales, this procedure will eventually lead to a pyramidal clustering of the fibers.

## 2 Method

The proposed top-down hierarchical fiber clustering scheme relies on multi-scale neuroanatomical fiber features, which will be detailed in Section 2.1. We will define in Section 2.2 the fiber similarity measure in the Mahalanobis distance, and introduce in Section 2.3 the hierarchy of the clustering algorithm.

### 2.1 Neuroanatomical Features of Fibers

Suppose that there are  $M$  ROIs, and the  $i$ -th entry  $\ell_i$  in the associativity vector  $L_a = (\ell_1, \ell_2, \dots, \ell_M)$  of fiber  $a$  indicates the spatial relationship of the fiber with the  $i$ -th ROI. Vector element  $\ell_i$  can be set to 1 if any segment of the fiber lies within the  $i$ -th ROI, and set to 0 otherwise. However, the binary formulation as such will result in sparse associativity vectors, pose challenges in estimating fiber distances, and increase the tendency of clustering algorithms to end in local minima.

Here, we propose a fuzzy associativity vector, which takes into account the diffusivity information provided by DTI. Recalling that a typical tractography algorithm traces fibers along the tensor eigenvectors corresponding to the largest eigenvalues, we mimic this process by diffusing each ROI along the fiber directions. Assume that a specific manually delineated ROI covers the domain  $\mathcal{L}$  with a constant mass concentration  $\phi(x) = \phi_c$ . The ROI would then automatically diffuse to the outside of  $\mathcal{L}$  due to the imbalance of concentration. We use a generic transport equation to characterize the diffusion of the ROI from  $\mathcal{L}$  to the image domain  $\Omega$ :

$$\nabla_t \phi + \eta(x)f(t, x, \phi, \nabla_x \phi) = g(t, x, \phi), \quad x \in \Omega - \mathcal{L}. \quad (1)$$

In general, the temporal changing rate of the concentration  $\nabla_t \phi$  is coupled with the concentration field  $\phi$  and its spatial changing rate  $\nabla_x \phi$ . The flux term  $f(\cdot)$  in Eq. 1 regulates the diffusion velocity by projecting the level-set norms of  $\phi$  onto the space formed by the local tensor  $T(x)$ :

$$f(t, x, \phi, \nabla_x \phi) = - \left( \frac{\nabla_x^* \phi}{\|\nabla_x^* \phi\|} \cdot T(x) \cdot \frac{\nabla_x \phi}{\|\nabla_x \phi\|} \right) \quad (2)$$

According to Eq. 2, the ROI diffuses rapidly where the norm of its surface is parallel to the eigenvector corresponding to the largest eigenvalue of the local tensor, i.e., coinciding with the fiber pathways. On the contrary, the diffusion would hardly happen if the surface norm of the ROI is nearly perpendicular to the fiber pathways. Meanwhile, the source term  $g(\cdot)$  in Eq. 1 enforces the boundary condition  $\phi|_{\partial \mathcal{L}} = \phi_c$ , preserving the surface ( $\partial \mathcal{L}$ ) of the manually delineated part ( $\mathcal{L}$ ) of the ROI. Further, as in tractography, only voxels whose FA values are sufficiently high (e.g.  $\geq 0.2$ ) are considered as possible fiber pathways. We have therefore introduced in Eq. 1 a window function  $\eta(\cdot)$  to exclude unrealistic ROI diffusion into low FA areas:

$$\eta(x) = \left( 1 + e^{-\alpha(\text{FA}(x) - \beta)} \right)^{-1} \quad (3)$$

The parameter  $\alpha$ , which controls the transition steepness of  $\eta(\cdot)$ , is set to 100 in our case. The center-of-transition cut-off FA value  $\beta$  is set lower than the minimal FA threshold in tractography (e.g. 0.15). The profile of  $\eta(\cdot)$  is dependent on the FA value. Fig. 1(b) gives a plot of  $\eta(\cdot)$  with  $\alpha = 100$  and  $\beta = 0.15$  and another with  $\alpha = 40$ .

An illustration of the ROI diffusion is given in Fig. 1(a), where the underlying tensor principal directions are displayed in green arrows. The zero level-set of the initial  $\phi$  (the dark blue circle) corresponds to the surface of the manually delineated ROI, and is designated as the start time  $t_0$ . The anisotropic diffusion is guided by the tensors. The boundary of the ROI surface gradually enlarges and finally deforms to the brown contour at the end time  $t_1$ . Also, for each voxel  $x$  in the diffused ROI, we define its *spatial confidence* as  $(1 - t_\tau)$ , based on the time  $t_\tau$  when the voxel  $x$  is traversed by the zero level-set of  $\phi$ . In Fig. 1(a) for example, voxels inside the dark-blue circle ( $t_0$ ) have a spatial confidence of 1, while the confidence gradually decreases to 0 at the brown contour ( $t_1$ ).

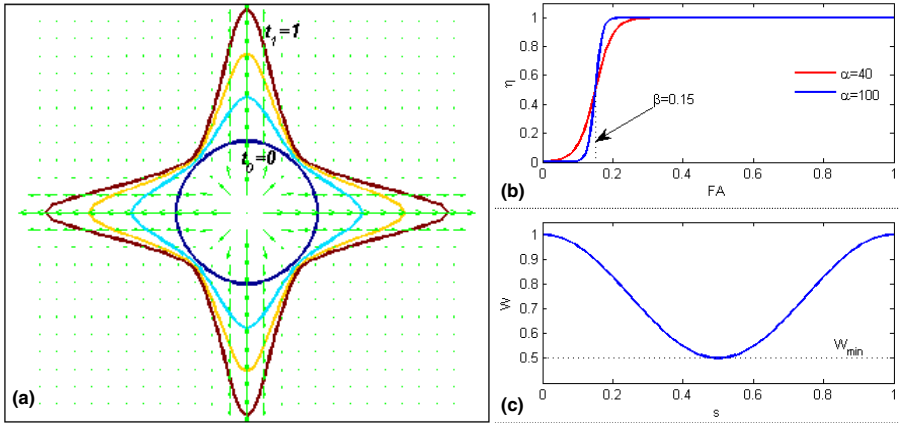


**Fig. 1.** An example of ROI diffusion is shown in (a), where the ROI surface gradually deforms from the dark-blue circle to the brown contour, guided by the underlying tensor principal directions indicated by green arrows. Panel (b) shows typical profiles of the window function  $\eta(\cdot)$  in Eq. 3. Panel (c) provides the importance distribution along the arc-length of the fiber, according to Eq. 4.

Given any fiber  $a$ , its *associativity* to the ROI under consideration is given by the maximal spatial confidence of the diffused ROI along the fiber. A fuzzy *associativity vector*  $L_a$  can thus be constructed with respect to all  $M$  ROIs, and is much less sparse compared to the binary formulation.

The end segments of a fiber are more important than the middle segments in fiber clustering [7]. By normalizing the fiber arc-length  $s$  to  $[0,1]$ , we can specify an *importance* weighting, in the range of  $[W_{\min}, 1]$ , to different points on the fiber:

$$\begin{aligned} W(s) &= \frac{1}{2}(1 - W_{\min})(1 + \cos 2\pi s) + W_{\min} \\ &= \cos^2 \pi s + W_{\min} \cdot \sin^2 \pi s \end{aligned} \quad (4)$$

A typical profile of  $W(s)$  is shown in Fig. 1(c), where the minimal importance  $W_{\min}$  is set to 0.5. It is worth noting that other forms of importance weighting (e.g., in [7]) are applicable here, since these weighting functions behave similarly by gaining higher importance for the end segments and lower in the middle.

With definition given in Eq. 4, the *importance* value of each ROI with respect to a fiber  $a$  can be acquired at the location where the corresponding *associativity* of the fiber  $a$  is picked. By considering all  $M$  ROIs, an *importance vector*  $W_a$  can be produced for each fiber  $a$ . Therefore, each fiber is characterized by two vectors – (i) the *associativity vector* carrying neuroanatomical features, and (ii) the *importance vector* weighting the respective neuroanatomical information.

### 2.2 The Mahalanobis Distance between Fibers

Good fiber clustering result is dependent on a good definition of fiber pairwise distance (or similarity). Pairwise distance between fibers can be computed based on the anatomical feature descriptors. A simple way is to view the associativity vectors as samples in the Euclidean space, where the norm and the inner-product are naturally defined. A better approach, however, is by taking into account the correlation of the ROIs in computing the fiber distance, since ROIs vary significantly in shape and size. By regarding the associativity vector of each fiber as an observation from a multivariate space [15], we can define a covariance matrix which relates the ROIs. Suppose  $L_a$  is the associativity vector for the fiber  $a$  ( $1 \leq a \leq N$ ) and  $(\cdot)^*$  is the transpose operator, the covariance matrix is:

$$C = \frac{1}{N} \sum_{a=1}^N C_a = \frac{1}{N} \sum_{a=1}^N \sqrt{L_a \cdot L_a^*} \tag{5}$$

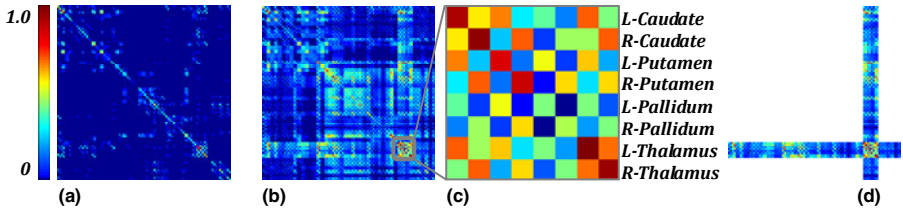


**Fig. 2.** Example covariance matrices on 90 ROIs are shown, using (a) binary and (b) fuzzy formulation of the associativity measures, respectively. Panel (c) is a close-up of the sub-cortical region in (b), where we can observe higher inside-hemisphere correlation than between-hemisphere. And (d) highlights the significant correlation between sub-cortical areas and other brain regions.

Fig. 2(a-b) give an example of the covariance matrices formed using 90 anatomical ROIs, based on the binary and the fuzzy associativity definitions, respectively. It is obvious that, with fuzzy associativity, the covariance matrix is denser, greatly reducing the sparseness of the associativity vectors. Zooming into the sub-cortical areas in Fig. 2(b), we could observe significant correlation within each hemisphere (Fig. 2(c)), as well as between sub-cortex and other anatomical regions (Fig. 2(d)), as suggested by [16].

Based on the covariance matrix of all ROIs defined in Eq. 5, the Mahalanobis distance between the fiber  $a$  and the fiber  $b$  can be calculated as follows:

$$d_M(a, b) = \sqrt{(L_a^* - L_b^*) \cdot \text{diag}(W_a \cdot W_b^*)^{\frac{1}{2}} \cdot \mathcal{C}^{-1} \cdot \text{diag}(W_a \cdot W_b^*)^{\frac{1}{2}} \cdot (L_a - L_b)} \quad (6)$$

Then, a corresponding similarity measure, which is to some extent more commonly used in clustering, can be define as  $s(a, b) = \exp(-d_M^2(a, b)/2\sigma^2)$ , where  $\sigma$  is a predefined value.

### 2.3 Multi-scale ROI and Hierarchical Clustering Framework

We have adopted a top-down hierarchical mechanism for more principled fiber clustering. In particular, an atlas with three sets of ROIs is registered and aligned to the image space of the DTI dataset. The three multi-scale sets of ROIs consist of 2 ROIs from the two hemispheres, 18 ROIs from various lobes, and finally 90 ROIs delineating different gyri and sulci of the brain [17]. In panel (a) of Fig. 3, we show the three sets of ROIs overlaid on the same typical cortical slice. The different sets of ROIs, therefore, provide information at different scales from the neuroanatomical perspective, giving multi-scale features which can be used to perform a 3-level hierarchical fiber clustering.

In the first level, based on the information given by the 2-ROI set, the tractography results can be easily grouped into 3 classes – fibers in two individual hemispheres and fibers bridging the two hemispheres. In the following two levels of the hierarchy, each class generated in the previous level is further divided into more subclasses, based on the anatomical information of fibers given by the corresponding set of diffused ROIs. As the neuroanatomical features relate to 18 and 90 ROIs in the last two levels, respectively, spectral clustering [18] is recursively called to further cluster fibers based on the similarity matrices of fibers.

Spectral clustering has been widely applied in fiber clustering [2][5], due to its high robustness and efficiency. And in spectral clustering, the number of classes is critical and has to be specified manually. For the convenience to demonstrate the proposed hierarchical fiber clustering method, we simply set the number of classes to 2 in each spectral clustering callback. There are reports in the literature designated to address the issue of optimal class number in spectral clustering [19]. However, the problem indeed exceeds the scope of our work in this paper, though methods to automatically determine the optimal number of classes can be easily integrated into the proposed hierarchical clustering framework.

## 3 Experimental Results

Fig. 3 shows the results given by the proposed method on approximately 12,000 fibers tracked using ExploreDTI [20] on an adult brain. As can be seen from the top of the figure, the fibers are first categorized at the first level of the hierarchical clustering into 3 classes – fibers in the left/right hemispheres and fibers connecting both hemispheres. In the second and third levels, these classes are further subdivided. We use the same color coding for hemispheric-symmetric fiber bundles. In the third level, the hierarchical clustering strategy yields a total of 12 bundles. And in all three levels, the intra-subject left-right-hemisphere symmetry is well preserved.

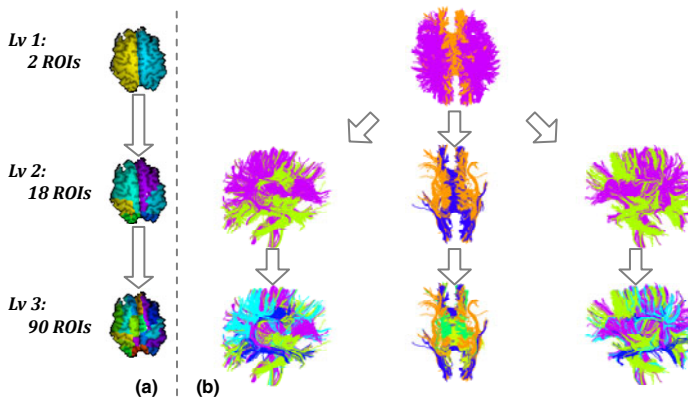


**Fig. 3.** Hierarchical fiber clustering is performed with the three sets of multi-scale ROIs shown in panel (a). With increasing levels of clustering, more subdivisions of the fibers are obtained, as shown in (b). To highlight the hemispheric symmetry, fiber clustering results in the two hemispheres are displayed in the same color coding.

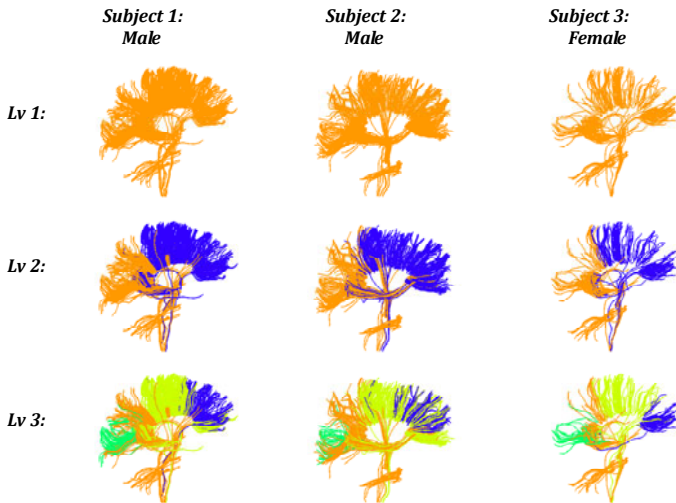


**Fig. 4.** Consistent fiber clustering across three adult subjects (2 males, 1 female). Here, for better visual inspection, only the fibers connecting the left and the right hemispheres are shown, with same color representing the corresponding bundles in different subjects.

We have further performed the proposed fiber clustering method on three adult brains. For better visualization, only the clustering results of fibers connecting two hemispheres are shown in Fig. 4. The first two subjects are male (~12,000 fibers), while the third one is female and has only ~6,000 fibers yielded by the same tractography algorithm with identical parameters. As we can observe, the inter-subject consistency of clustering is still achieved, due to the use of neuroanatomical information in guiding fiber clustering.

## 4 Conclusion

We have presented in this paper a hierarchical fiber clustering method. In each level of the hierarchical clustering, our method leverages atlas-based information provided by ROI set of the specific scale. In particular, fuzzy anatomical associativity for each fiber is acquired from the set of diffused ROIs, together with the fiber geometry related importance weighting. The Mahalanobis pairwise distance between fibers is then computed and fed into a spectral clustering algorithm in pyramidal fashion, for performing fiber clustering. Experimental results show that the proposed method obtains good intra-subject symmetry and inter-subject consistency.

## References

- [1] Ding, Z., Gore, J.C., Anderson, A.W.: Classification and Quantification of Neuronal Fiber Pathways Using Diffusion Tensor MRI. *Magnetic Resonance in Medicine* 49, 716–721 (2003)
- [2] Brun, A., Knutsson, H., Park, H.-J., Shenton, M.E., Westin, C.-F.: Clustering Fiber Traces Using Normalized Cuts. In: Barillot, C., Haynor, D.R., Hellier, P. (eds.) *MICCAI 2004*. LNCS, vol. 3216, pp. 368–375. Springer, Heidelberg (2004)
- [3] Gerig, G., Gouttard, S., Corouge, I.: Analysis of Brain White Matter Via Fiber Tract Modeling. In: *IEEE EMBS 2004*, vol. 2, pp. 4421–4424 (2004)
- [4] Corouge, I., Gouttard, S., Gerig, G.: Towards a Shape Model of White Matter Fiber Bundles Using Diffusion Tensor MRI. In: *ISBI 2004*, vol. 1, pp. 344–347 (2004)
- [5] O'Donnell, L., Westin, C.-F.: White Matter Tract Clustering and Correspondence in Populations. In: Duncan, J.S., Gerig, G. (eds.) *MICCAI 2005*. LNCS, vol. 3749, pp. 140–147. Springer, Heidelberg (2005)
- [6] Jonasson, L., Hagmann, P., Thiran, J.-P., Wedeen, V.J.: Fiber Tracts of High Angular Resolution Diffusion MRI are Easily Segmented with Spectral Clustering. In: *ISMRM 2005* (2005)
- [7] Klein, J., Bittihn, P., Ledochowitsch, P., Hahn, H.K., Konrad, O., Rexilius, J., Peitgen, H.-O.: Grid-based Spectral Fiber Clustering. In: *SPIE Medical Imaging 2007*, vol. 6509 (2007)
- [8] Maddah, M., Zollei, L., Grimson, W.E.L., Wells, W.M.: Modeling of Anatomical Information in Clustering of White Matter Fiber Trajectories Using Dirichlet Distribution. In: *MMBIA 2008* (2008)
- [9] Maddah, M., Grimson, W.E.L., Warfield, S.K., Wells, W.M.: A Unified Framework for Clustering and Quantitative Analysis of White Matter Fiber Tracts. *Medical Image Analysis* 12(2), 191–202 (2008)
- [10] Wang, X., Grimson, E., Westin, C.-F.: Tractography Segmentation Using a Hierarchical Dirichlet Processes Mixture Model. In: Prince, J.L., Pham, D.L., Myers, K.J. (eds.) *IPMI 2009*. LNCS, vol. 5636, pp. 101–113. Springer, Heidelberg (2009)
- [11] Maddah, M., Mewes, A.U.J., Haker, S., Grimson, W.E.L., Warfield, S.K.: Automated Atlas-Based Clustering of White Matter Fiber Tracts from DTMRI. In: Duncan, J.S., Gerig, G. (eds.) *MICCAI 2005*. LNCS, vol. 3749, pp. 188–195. Springer, Heidelberg (2005)
- [12] Xia, Y., Turken, A.U., Whitfield-Gabrieli, S.L., Gabrieli, J.D.: Knowledge-Based Classification of Neuronal Fibers in Entire Brain. In: Duncan, J.S., Gerig, G. (eds.) *MICCAI 2005*. LNCS, vol. 3749, pp. 205–212. Springer, Heidelberg (2005)

- [13] O'Donnell, L., Westin, C.-F.: Automatic Tractography Segmentation Using a High-Dimensional White Matter Atlas. *IEEE Trans. Medical Imaging* 26(11), 1562–1575 (2007)
- [14] Li, H., Xue, Z., Guo, L., Liu, T., Hunter, J., Wong, S.T.C.: A Hybrid Approach to Automatic Clustering of White Matter Fibers. *NeuroImage* 49(2), 1249–1258 (2010)
- [15] Gong, G., He, Y., Concha, L., Lebel, C., Gross, D.W., Evans, A.C., Beaulieu, C.: Mapping Anatomical Connectivity Patterns of Human Cerebral Cortex Using In Vivo Diffusion Tensor Imaging Tractography. *Cerebral Cortex* 19(3), 524–536 (2008)
- [16] Hagmann, P., Cammoun, L., Gigandet, X., Meuli, R., Honey, C.J., Wedeen, V.J., Sporns, O.: Mapping the Structural Core of Human Cerebral Cortex. *PLoS Biology* 6(7), 1479–1493 (2008)
- [17] Tzourio-Mazoyer, N., Landeau, B., Papathanassiou, D., Crivello, F., Etard, O., Delcroix, N., Mazoyer, B., Joliot, M.: Automated Anatomical Labeling of Activations in SPM Using a Macroscopic Anatomical Parcellation of the MNI MRI Single-Subject Brain. *NeuroImage* 15(1), 273–289 (2002)
- [18] Shi, J., Malik, J.: Normalized Cuts and Image Segmentation. *IEEE Trans. Pattern Analysis and Machine Intelligence* 22(8), 888–905 (2000)
- [19] Xiang, T., Gong, S.: Spectral Clustering with Eigenvector Selection. *Pattern Recognition* 41(3), 1012–1029 (2008)
- [20] Leemans, A., Jeurissen, B., Sijbers, J., Jones, D.K.: ExploreDTI: A Graphical Toolbox for Processing, Analyzing, and Visualizing diffusion MR Data. In: *ISMRM 2009* (2009)